J Solid State Electrochem (2001) 5: 487–494
DOI 10.1007/s100080100193

ORIGINAL PAPER

Tomáš Grygar · Petr Bezdička · Pawel Piszora
Emilia Wolska

Electrochemical reactivity of Li–Mn–O and Li–Fe–Mn–O spinels

Received: 3 September 2000 / Accepted: 12 January 2001 / Published online: 13 June 2001

Abstract Electrochemical reductive dissolution of Li–Mn–O and Li–Fe–Mn–O spinels and Li^+ extraction/insertion in these oxides were performed using voltammetry of microparticles. Both electrochemical reactions are sensitive to the Fe/(Fe + Mn) ratio, specific surface area, Li content in tetrahedral positions, and Mn valence, and can be used for electrochemical analysis of the homogeneity of the elemental and phase composition of synthetic samples. The peak potential (E_P) of the reductive dissolution of the Li–Mn–O spinel is directly proportional to the logarithm of the specific surface area. E_P of Li–Fe–Mn–O spinels is mainly controlled by the Fe/(Fe + Mn) ratio. Li^+ insertion/extraction can be performed with Mn-rich Li–Fe–Mn–O spinels in aqueous solution under an ambient atmosphere and it is sensitive to the regularity of the spinel structure, in particularly to the amount of Li in tetrahedral positions and the Mn valence.

Keywords Li–Mn–O spinel · Dissolution · Li insertion

Introduction

Several Li–Mn–O spinels [1], $LiFe_5O_8$, and their solid solutions (Fig. 1) were studied in the system Li–Fe–Mn–O, such as $Li_{4/3}Mn_{5/3}O_4$–$LiFe_5O_8$ [2], $Li_{0.5}(Fe,Mn)_{2.5}O_4$ [2, 3, 4], $LiMn_2O_4$–$LiFe_5O_8$ [5, 6], and others [7]. Spinels with sufficient Fe are ferrimagnetic with a Curie temperature above room temperature and evoked interest in their magnetic properties [2]. The spinels have cubic *Fd*3*m* symmetry in spite of a high Mn^{III} content [2], and Fe-rich spinels exhibit ordering of Li and Fe in octahedral positions, leading to $P4_332$ symmetry. The ionic distribution of metals in the spinel lattice follows several rules. Li occupies all tetrahedral positions in $LiMn_2O_4$ and is exclusively present in octahedral positions in $Li_{0.5}Fe_{2.5}O_4$, but the Li occupation does not follow a simple linear dependence on the Fe/(Fe + Mn) ratio [2, 4, 5, 6]. Nonstoichiometric Li–Fe–-Mn-O spinels are formed when the Li/(Fe + Mn) ratio changes as shown in the triangular diagram in Fig. 1. In addition, the Mn valence is a function of the redox conditions during the synthesis. Beside the Li–Fe–Mn–O spinel desired, phase impurities are formed from the excess metals, such as Mn_3O_4 [2], Li_2MnO_3 [4], $LiMn_2O_4$ [3, 8, 9], and $MnFe_2O_4$ [9], usually with X-ray diffraction (XRD) patterns similar to the main component.

Li–Mn–O spinels have exceptional electrochemical properties related to a highly reversible Li^+ insertion/extraction reaction that proceeds in both aqueous and nonaqueous solutions. $LiMn_2O_4$ and its delithiated product, λ-MnO_2, have been proposed as sorbents [10], an ion-selective electrode for Li^+ [11], and as an electrode material for Li^+ batteries [12, 13, 14]. All these applications are based on either chemical (Eq. 1) or electrochemical (Eq. 2) reactions:

$$LiMn_2O_4 + 1/4O_2 + H^+ \rightarrow Li^+ + 2\lambda - MnO_2 + 1/2H_2O, \quad (1)$$

$$LiMn_2O_4 \rightarrow Li^+ + e^- + \lambda - MnO_2. \quad (2)$$

The latter reaction proceeds not only in organic solvents, but also in aqueous solutions in the presence of Li^+ [11, 14]. A further possible reaction of the Mn spinel, its dissolution, can be an unwanted phenomenon in these cases. Reductive dissolution can be expressed by Eq. (3).

$$LiMn_2O_4 + 3e^- + 8H^+ \rightarrow Li^+ + 2Mn^{2+} + 4H_2O \quad (3)$$

We recently studied electrochemical dissolution of several Mn oxides including pure $LiMn_2O_4$ [15] using

Presented at the international conference "Solid State Chemistry 2000"; 3–8 September 2000, Prague, Czech Republic

T. Grygar (✉) · P. Bezdička
Institute of Inorganic Chemistry, 250 68 Řež, Czech Republic
E-mail: grygar@iic.cas.cz

P. Piszora · E. Wolska
Adam Mickiewicz University, Grunwaldzka 6,
60 780 Poznan, Poland

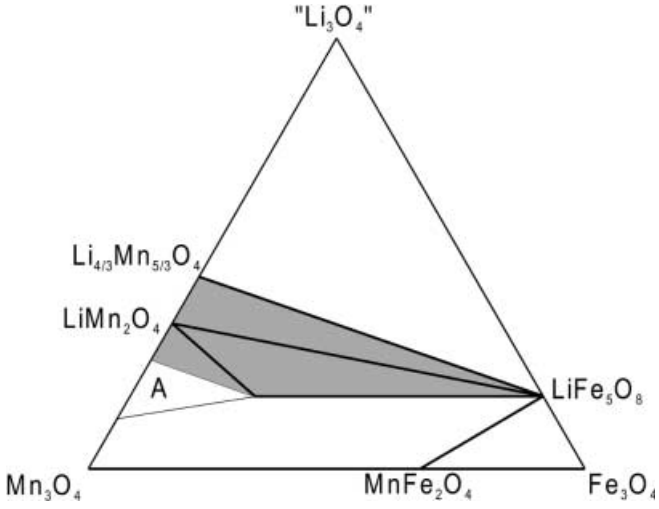

Fig. 1 Triangular diagram of Li–Fe–Mn–O spinels [2, 7]. The *inner lines* stand for spinel solid solutions. The vacant triangle *A* surrounding the hypothetical phase $LiMn_5O_8$ is a region where no single-phase spinels occur

voltammetry of immobilized microparticles [16]. In this technique the working electrode is prepared by mechanical attachment of electroactive particles on the surface of, for example, a graphite rod. The reaction is not adversely affected by slow mass transport phenomena as in the case of macroscopic films [17] or composite oxide electrodes made of the solid to be studied, carbon, and binder [18]. Recently other techniques, which have been based on a single particle [19] or more particles [20] embedded into a metallic electrode, have been used to avoid utilization of additives and decrease ohmic drops. However, voltammetry of microparticles remains the most used method for the direct electrochemical study of powdered compounds.

Substitution of Mn by other metals is used to alter the electrochemical properties of the electrode materials based on Mn oxides. The question therefore arises of what the relationship between electrochemical reactivity and substitution of Mn by other metal ions is. Such a question can only be answered by a study of the reactivity of well-defined mixed oxides, because there is no theory to predict the properties of substituted metal oxides. Solid solution $LiMn_2O_4$–$Li_{0.5}Fe_{2.5}O_4$ has recently been synthesized and characterized by Wolska and coworkers [5, 6, 21]. This allowed us to present the study of the influence of the electrochemical properties of these mixed oxides on their electrochemical reactivity according to Eqs. (2) and (3). A systematic study of the Li–Fe–Mn–O spinels enabled us to further test the phenomenology and analytical capability of voltammetry of immobilized microparticles.

Experimental

Synthesis

The synthesis of the solid solutions $LiMn_2O_4$–$Li_{0.5}Fe_{2.5}O_4$, denoted series S, was described in our previous reports [5, 6, 21]. Samples of solid solutions with the composition $(1-x)LiMn_2O_4{\cdot}xLi_{0.5}Fe_{2.5}O_4$ were prepared from mixtures of iron–manganese oxide precursors with molar ratio Fe/(Fe + Mn) = 0.0–1.0. These oxide precursors were obtained by autoclaving the coprecipitated amorphous Fe(III)Mn(II) hydroxides at 150 °C for 7 days. The structure of the Mn/Fe precursors changed successively, with the increase in the Fe/(Fe + Mn) ratio, from the tetragonal hausmannite (Mn_3O_4) through the cubic spinel $MnFe_2O_4$ to the hexagonal, Mn-doped hematite (α-Fe_2O_3). The precursors were then heated with the appropriate quantities of Li_2CO_3 for 4 h in air at a temperature increasing from 600 to 850 °C with the increase in Fe content.

The samples of Li–Fe–Mn–O spinels and undoped Li–Mn–O spinels, denoted series C, were synthesized by the citrate method described in Ref. [15]. The solution of corresponding metal nitrates and citric acid in a minimal amount of water was evaporated to a dry foam that was fired at about 400 °C and calcined at the desired temperature in air. The molar amount of citric acid must be about two-thirds of the molar amount of nitrates to avoid blazing of the dry foam [15, 19]. The phase purity of the spinels was checked by XRD, and the elemental composition was confirmed by chelatometric titration, emission spectrometry, and iodometry. For the comparison we also prepared Li–Mn–O spinels (series U) by the self-combustion method based on evaporation of metal nitrates and urea and ignition of the residue as described in Ref. [23]. The actual molar amount of urea-to-nitrate ions was 1:2. One sample of the Li–Mn–O spinels was prepared by evaporation of Li and Mn nitrates on a hot plate and calcination of the solid residue (series N). The final calcination temperatures, cubic lattice parameters, specific surface areas, and mean Mn valence in the Li–Mn–O spinels are summarized in Table 1.

Table 1 Description of Li–Mn–O spinel samples and their electrochemical characteristics. T_{CALC}: final calcination temperature, a: lattice parameter, σ: specific surface area, E_P: peak potential of the reductive dissolution, I_{P1}, I_{P2}, and I_{MIN}: characteristic currents of the anodic branch of Li^+ insertion/extraction reaction according to Fig. 3A. For denotation of the sample series (C, N, and U) see Experimental

Sample	T_{calc} (°C)	a (nm)	σ (m^2/g)	Mn valence	Dissolution	Li^+ extraction		
					E_P *(V versus SCE)*	I_{P1} (μA)	I_{P2} (μA)	$-I_{MIN}$ (μA)
C661	800	0.825	4.3	3.50	0.40	229	191	164
C5510	1,000	0.824	0.42	3.42	0.34	90	96	56
C5516	900	0.825	0.68	3.51	0.36	108	136	74
N748	400	0.819	1.52	3.64	0.37	76	79	0
N749	400	0.816	1.92	3.67	0.36	63	66	6
C7110	600	0.821	21.3	3.52	0.46	104	147	71
U848	600	0.823	11.7	3.53	0.45	135	181	51
U849	600	0.823	13.8	3.60	0.45	87	115	14
U8410	600	0.822	17.1	3.64	0.45	145	192	19

Characterization

XRD was performed with a Siemens D5005 instrument (Cu Kα radiation, 40 kV, 30 mA, diffracted beam monochromator). Qualitative analysis was performed with Bede ZDS for Windows, version 1.99. For quantitative analysis of the XRD patterns we used PowderCell for Windows, version 2.3. The specific surface area was determined by single-point Brunauer–Emmett–Teller adsorption isotherms with a Coulter SA3100. The elemental composition was determined by atomic absorption spectroscopy (Fe, Mn), chelatometric titration (Mn), and emission spectrometry (Li). The Mn valence was determined by iodometry (Li–Mn–O spinels) or dissolution in ferrous sulfate solution followed by titration with permanganate (Li–Fe–Mn–O spinels).

Electrochemistry

Voltammetry was performed with a μAutolab potentiostat controlled by the GPES 4.4 program, both provided by EcoChemie (Utrecht, The Netherlands). The samples were deposited by intensive rubbing of a pile of sample on filter paper with a paraffin-impregnated graphite working electrode. A saturated calomel electrode (SCE) was used as a reference and a Pt plate as a counterelectrode. For Li^+ insertion/extraction, cyclic voltammetry was applied at a 10-mV/s scan rate between –0.5 and 1.2 V/SCE in 1 M LiCl. For reductive dissolution, linear sweep voltammetry at a 1-mV/s scan rate from the open-circuit potential to –0.8 V and 0.2 M acetic acid–acetate buffer (1:1) were used.

Results

Sample synthesis and characterization

After heating the precursors of series S in air with Li_2CO_3, crystalline solid solutions of nominal composition $LiMn_2O_4$–$Li_{0.5}Fe_{2.5}O_4$ were formed displaying exclusively a spinel structure. In samples with $Fe/(Fe+Mn) > 0.7$ the ordering of Li^+ in the octahedral spinel sublattice causes the lowering of the crystal symmetry to the cubic primitive unit cell (1:3 ordered spinel) [5]. The samples of Li–Mn–O spinels, series C, were finely crystalline spinels with a specific surface area between 0.5 and 20 m^2/g (Table 1). The specific surface area was inversely proportional to the final calcination temperature and was similar for the products obtained by a significantly more complicated version of the citrate route [24]. The Mn valence in the Li–Mn–O spinels, series C, ranged from 3.4 to 3.7 (Table 1) depending on the Li/Mn ratio and heating temperature [1]. The Mn valence (Table 2) from 3.0 to 3.7 in samples of Li–Fe–Mn–O spinels of series C was controlled by the appropriate Li/(Fe + Mn) ratio. The highest theoretical Mn valence in Li spinels, i.e., 4, can be achieved neither in Li–Mn–O spinels [1, 8] nor in Li–Fe–Mn–O spinels [2]. The actual amount of Li in the Li–Mn–O spinels was 0.38–0.45 per Mn. As shown in Fig. 1, the spinels, in which the Mn valence exceeded 3.5 of the stoichimetric $LiMn_2O_4$, had lattice parameters lower than the 0.824 nm expected for the stoichimetric phase [1]. Both facts indicate that majority of the Li–Mn–O spinels studied lay on the line connecting $LiMn_2O_4$ and λ-MnO_2 in the phase diagram published by Le Cras et al. [1].

Table 2 Fe concentration, Mn valence, and reductive peak potentials of single-phase Li–Fe–Mn–O spinels. For denotation of the sample series (S and C) see Experimental

	Fe/(Fe + Mn)	Li/(Fe + Mn)	Mn valence	Ep (V versus SCE)
S01	0.1	0.47		0.17
S02	0.2	0.44		0.05
S03	0.3	0.41		0.01
S04	0.4	0.38		–0.07
S05	0.5	0.35		–0.35
S06	0.6	0.32		–0.41
S07	0.7	0.29		–0.42
S08	0.8	0.26		–0.50
S09	0.9	0.23		–0.60
S10	1.0	0.20		–0.70
C1053	0.29	0.18	3.01	–0.26
C1055	0.29	0.22	3.12	–0.15
C1051	0.38	0.46	3.70	–0.24
C961	0.48	0.17	2.97	–0.29
C962	0.48	0.20	3.11	–0.33
C1071	0.74	0.30	3.50	–0.49
C1072	0.77	0.34	3.65	–0.58
C1073	0.77	0.30	3.47	–0.54

Probably owing to the much more exothermic, almost explosive course, the products resulting from the urea nitrate self-combustion technique contained a 2–5% admixture of bixbyite, C-Mn_2O_3. In contrast, using the citrate method, the dry foam turned dark and carbonized without blast. It was not necessary to add other additives to the reaction mixture, as was required in Ref. [24]. The carbonized grayish-black ash was then calcined at the controlled temperature in air. Using both the citrate and the urea nitrate routes we observed that if the temperature at any intermediate stage increased above the limit of stability of the desired products, crystalline byproducts were formed and the time necessary for the final calcination increased significantly.

The phase purity of the solids was evaluated by powder XRD. To get more detailed information in the case of Li–Fe–Mn–O spinels, the XRD patterns were processed using PowderCell to compare the calculated and measured diffraction patterns to reveal possible traces of phase impurities. We founded that the members of series S with $x = 0.5$ and $x = 0.6$ showed a certain line broadening of diffraction lines at bigger angles, such as (440), or small satellite peaks. This fact could easily be overlooked without careful XRD measurement and data processing. It might indicate a low percentage of an admixture of the phases with a structure similar to those of the main component, or tetragonal distortion of the spinel lattice reported by Endres et al. [8].

The presence of traces of monoclinic Li_2MnO_3 has already been reported in Li–Fe–Mn–O spinel samples [4] with the desired composition $LiFe_5O_8$–$LiMn_2O_4$ at $Fe/(Fe + Mn) > 0.7$. We obtained a low percentage of an admixture of this phase in similar samples of series C. In two samples with lower amount sof Fe and Li we found about 30% admixture of the tetragonal spinel with $a \sim 5.78$ Å and $c \sim 9.15$ Å. This phase might be identical to the "hausmanite structure" of the product with

Li/(Fe + Mn) = 0.5 and Fe/(Fe + Mn) = 0.2 reported by Blasse [2] without further details. In one case we found a bixbyite admixture. The amount of impurities in the samples did not exceed 5%.

Electrochemistry

Li^+ insertion/extraction reaction

Li^+ insertion/extraction proceeds without dissolution of the spinels in solutions with sufficient excess Li^+ over H^+. Usually, neutral or alkaline solution with 10^{-1}–10 M Li^+ is used. The reaction is frequently denoted as a 4-V process in the literature on batteries. In both aqueous and nonaqueous solutions, the reaction consists of two steps [11, 12, 13, 14, 20, 24, 25]. As a result, there are two maxima on both the anodic and cathodic branches of the cyclic voltammetric curves of the nonsubstituted Li–Mn–O spinels (Figs. 2, 3). Also square-wave voltammetry and chronoamperometry confirm the two-step reaction course (not shown here). The reason for the two-step reaction mechanism has not been identified, but it might be related to some phase transition in the series $LiMn_2O_4$–MnO_2, such as the discontinuity in the XRD spectra described by Kanamura et al. [26]. The actual shape of the cyclic voltammetric curves changes from sample to sample according to their varying crystallinity [11, 12, 24]. We processed the anodic branch of the cyclic voltammetric curves of the spinels according to Fig. 3A, using Eq. (4):

$$G = 2I_{MIN}/(I_{P1} + I_{P2}). \quad (4)$$

G can have values between 0 and 1, where 0 means no current minimum on the anodic branch of the voltammetric curve. We compared G of nine samples of nonsubstituted Li–Mn–O spinels to their specific surface, processing temperature, and average Mn valence (Table 1). We found the best correlation with the last parameter (Fig. 3B): the higher the Mn valence, the lower the separation of the two extraction steps. Higher values of the Mn valence are typical for the samples synthesized at lower temperatures [1, 8], and accordingly the low-temperature samples were reported to yield voltammetric curves without the current minimum in nonaqueous solution [24]. Accordingly, Le Cras et al. [1] stated that 600 °C is the lowest temperature at which the regular structure of $LiMn_2O_4$ develops.

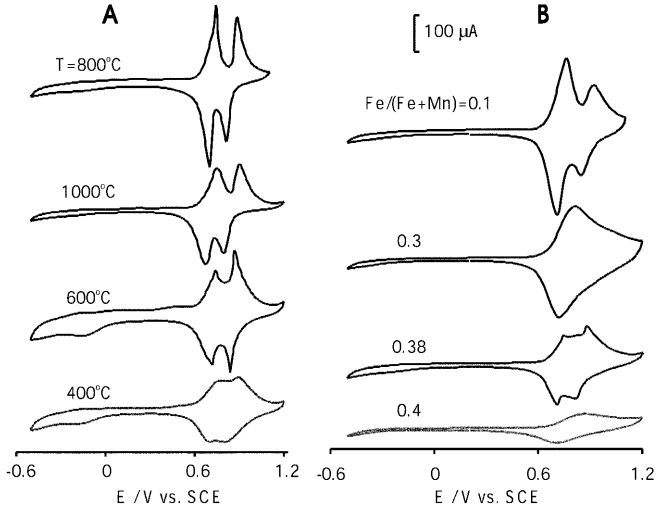

Fig. 2A, B The voltammetric curves of the Li^+ insertion/extraction reaction according to Eq. (2). Conditions: 1 M LiCl, 10 mV/s, fourth scans. **A** Voltage-current curves of nonsubstituted samples. The final calcination temperature is given on the curves **B** Voltage-current curves of Li–Fe–Mn-O spinels. The Fe/(Fe + Mn) ratio is given on the curves

As demonstrated in Fig. 2B, owing to substitution of Mn by Fe the peak shape of the Li^+ insertion reaction was changed. The current of the more positive peak decreased, and the originally double peak coalesced to a single peak, $G = 0$, at Fe/(Fe + Mn) > 0.2. The same change was reported for Li,Fe,Mn spinel in a nonaqueous environment [27]. The disappearance of the two-stepped nature of the reaction is also visible in square-wave voltammograms. Similarly Kawai et al. [28] observed the disappearance of the more positive Li^+ extraction step in $LiCo_xMn_{2-x}O_4$ at x = 0.4. With Fe/(Fe + Mn) growing above 0.3, there was a dramatic decrease in the overall spinel reactivity. In the two neighboring samples of series S with Fe/(Fe + Mn) = 0.3 and 0.4 the Li^+ content in the tetrahedral position changes from 95 to 68%, respectively [6]. Such a sharp change of Li^+ preference to octahedral and tetrahedral positions is common in approximately half of the series of solid solutions of Li–Fe–O and Li–Mn–O spinels [2]. The electroactivity of the samples with Fe/(Fe + Mn) > 0.4 to the Li^+ insertion/extraction reaction was negligible. We can therefore conclude that only Li^+ (or vacancies after Li^+ extraction) of tetrahedral positions can be electrochemically extracted and that this is valid only when the content of these active sites is close to 100% of all the tetrahedral sites available in stoichiometric spinel.

With the potential applied and the supporting electrolyte used, we did not observe the second Li^+ insertion into $LiMn_2O_4$ producing $Li_2Mn_2O_4$ that can also proceed in nonaqueous [13] and aqueous [14] solutions.

Electrochemical dissolution

Electrochemical reductive dissolution of particulate Mn oxides [15, 31] and Fe oxides [32] in slightly acidic solution can be conveniently followed by voltammetry. The reaction is irreversible. The dissolution of Li–Fe–Mn–O spinels can be expressed by Eq. (5):

$$Li_{1-x/2}Mn_{2-2x}Fe_{2.5x}O_4 + (3 - 0.5x)e^- + 8H^+ \rightarrow (1 - x/2)Li^+ + (2 - 2x)Mn^{2+} + 2.5xFe^{2+} + 4H_2O. \quad (5)$$

Both the reaction products Mn^{2+} and Fe^{2+} are sufficiently soluble in moderately acidic solutions to allow

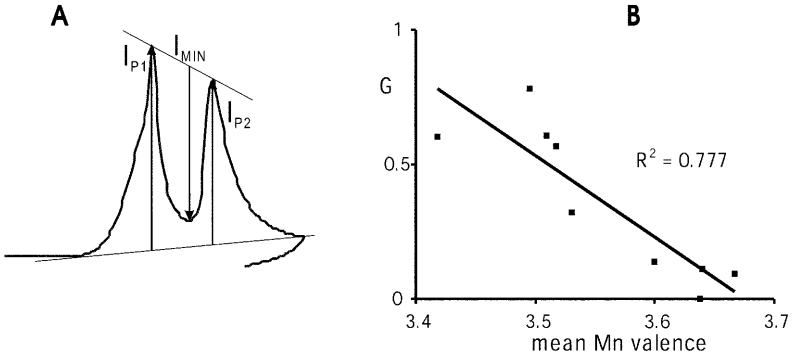

Fig. 3 **A** Currents I_{P1}, I_{P2}, and I_{MIN} used to characterize the shape of the anodic voltammetric curve of the Li^+ insertion/extraction reaction (see Eq. 4) **B** Dependence between $G = 2I_{MIN}/(I_{P1} + I_{P2})$ and average Mn valence

total consumption of the solids. Because the particle size of the samples was less than 1 μm, a complete dissolution was achieved during the first scan at a scan rate of 1 mV/s. We did not observe the complicated reaction course reported for much thicker MnO_2 layers [17]. As a result of a simple reaction mechanism, the dissolving Li–Mn–O- and Li–Fe–Mn–O spinels yielded simple voltammetric peaks of which the peak potentials (E_P) could be easily determined.

The dependence between the voltammetric curves and the physical and chemical properties of the powdered reactants was discussed elsewhere [32], where we showed that E_P depends significantly on the phase composition and the particle size of the powder. The bigger the particle size, the more negative the peak of the electrochemical reduction of the powder reactant of the same phase composition. The actual influence of the specific surface, σ, on the E_P is demonstrated in Fig. 4 for all the Li–Mn–O spinel samples synthesized for this work. The slope of E_P versus $\ln(\sigma)$ is 32 mV. The theory predicts this slope to be $RT/\alpha nF$ [32, 33]. The mechanism of the reductive dissolution of Mn oxides is rather complex [15, 17], and so the meaning of αn is rather formal. The effective value of $\alpha nF/RT$ of about 15 was observed at the peak potentials of $LiMn_2O_4$ dissolution [15] and hence the actual slope of E_P versus $\ln(\sigma)$ is about half of the predicted value, but the experimental dependence in Fig. 4 is statistically significant ($r^2 = 0.94$, $n = 10$).

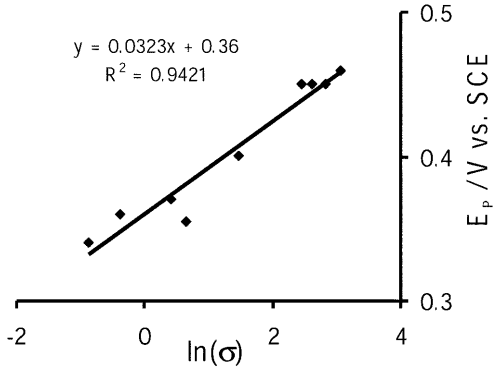

Fig. 4 Peak potential of reductive dissolution of Li–Mn–O spinel versus natural logarithm of specific surface area. Conditions: acetate buffer, the first scan from open-circuit potential (about 0.5 V versus SCE) cathodically, scan rate 1 mV/s

The electrochemical reactivity of mixed oxides commonly depends on the level of substitution of the electroactive metal ion [29, 30]. The continuous series of Li–Mn–O spinels and $LiFe_5O_8$ offers a unique example of the continuous change of the ratio of two electroactive ions with different reactivity in the single crystal structure. The difference in reactivity of spinels with various Fe/(Fe + Mn) is apparent from Fig. 5. In Fig. 5B, the dissolution peak potentials of Li–Fe–Mn–O spinels of series S and C are plotted against the molar ratio of Fe. The shift of the cathodic peak potentials with increasing content of Fe is as large as 1 V in the whole series. Because the reactants are solid solutions, there is a single voltammetric peak and not two peaks, one corresponding to the dissolution via Mn(III,IV) reduction and the other to Fe(III) reduction. There is no general rule for such evaluation of electrochemical reactivity, for example, similar to the Vegard rule in structural chemistry, but we can refer to an analogy with the peak potential of solid solutions of AgCl–AgBr [34], Ni–Fe [35], and Cu–Fe hexacyanoferrates [36]. In the solid solution Li–Fe–Mn–O spinels there is an almost linear dependence of E_P on the content of Fe; this resembles such dependences for AgCl/AgBr [34] and cyanoferrates [35]. In the case presented the dependence in Fig. 5B is also valid for samples with different mean Mn valence (cf. Table 2). In contrast, Li^+ insertion/extraction in $LiCo_xMn_{2-x}O_4$ consists of two separate steps corresponding to Mn^{III}/Mn^{IV} and Co^{III}/Co^{IV} cycling [28].

It was already shown that voltammetry could reveal heterogeneity of the composition or crystallinity of the electroactive powders [30, 37, 38, 39]. We therefore intentionally prepared several samples of Li–Fe–Mn–O spinels with heterogeneous phase composition. Outside the range of stability of the spinel solid solutions in Fig. 1, the structural heterogeneity first distorts the shape of the XRD diffraction lines at bigger angles, which is, however, visible only after careful data examination. With further increasing nonstoichiometry of the reacting mixture, additional oxide species can be unequivocally distinguished in the XRD pattern. In certain cases even the first stage of heterogeneity can be revealed from the increasing width of a voltammetric dissolution peak or the peak splitting. This indications can be especially valuable in the case of Fe-rich members of series $Li_{0.5}(Fe_xMn_{1-x})_{2.5}O_4$ with the lattice parameter a lying

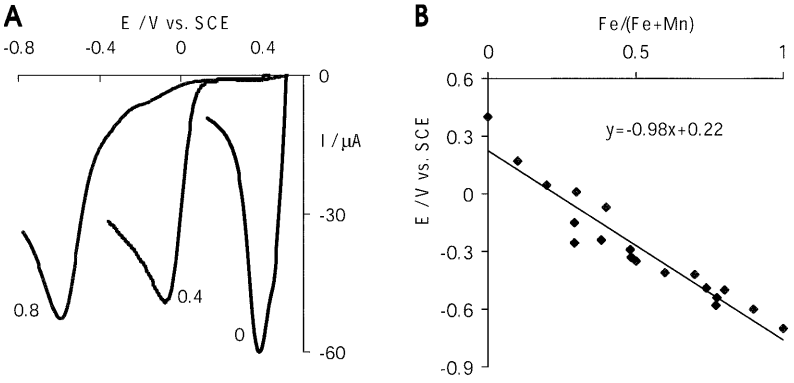

Fig. 5 **A** Voltammetric dissolution curves of several single-phase Li–Fe–Mn–O spinels of series S. The *numbers* denotes the value Fe/(Fe + Mn). Conditions: as in Fig. 4. **B** Voltammetric peak potentials of single-phase Li–Fe–Mn–O spinels of series S and C plotted against Fe/(Fe + Mn)

in a very narrow range between 8.33 and 8.35 Å at $0.7 < Fe/(Fe + Mn) < 1$ [2] or for $LiMn_2O_4$–$Li_{0.5}Fe_{2.5}O_4$ with *a* between 8.30 and 8.33 Å at $0.6 < Fe/(Fe + Mn) < 1$ [5]. An additional disadvantage of the XRD analysis of the homogeneity of the samples is that the actual lattice parameter of Li–Mn–O spinels depends on the heating temperature, which mainly affects Mn valence and actual value of Li/(Li + Mn) [1, 8, 24]. All these influences worsen the applicability of the XRD analysis to evaluate the spinel uniformity. An example of the sensitivity of voltammetry is shown in Fig. 6. Two samples, C961 and C965, had different Li/(Fe + Mn) ratios, but whereas C961 was uniform according to XRD and voltammetry, the diffraction lines of C965 were broadened and with minor satellite peaks close to (511), (440), and (531). XRD analysis could not unequivocally identify the two (or more) spinels, but voltammetry clearly revealed two species with a peak separation of 0.33 V, which, according to Fig. 5B, corresponds to two spinels with an Fe/(Fe + Mn) ratio difference of about 0.3. We observed such peak splitting in several other samples, where the XRD diffraction peaks usually also consisted of overlapped diffractions of similar spinels, especially at Fe/(Fe + Mn)~0.5. If we alternatively had explained the XRD line broadening by tetrahedral distortion of the spinel lattice [8], we would not have observed the split voltammetric peak.

The phase admixtures formed beside the cubic spinels according to XRD analysis were Li_2MnO_3, the tetragonal spinel mentioned previously, and bixbyite, C-Mn_2O_3. The two latter oxides are also reductively dissolved and can therefore be detected by voltammetry, if the actual Fe/(Fe + Mn) ratio of the mixture components differs by more than about 0.1, which corresponds to more than 0.1-V separation of the volammetric peaks. The reactivity of Fe-doped bixbyite is described elsewhere [31]. Examples of voltammetric curves of samples with phase admixtures are shown in Fig. 6. Mn_3O_4 obtained by calcination at temperatures about 1000 °C was not electrochemically reductively dissolved under the conditions applied.

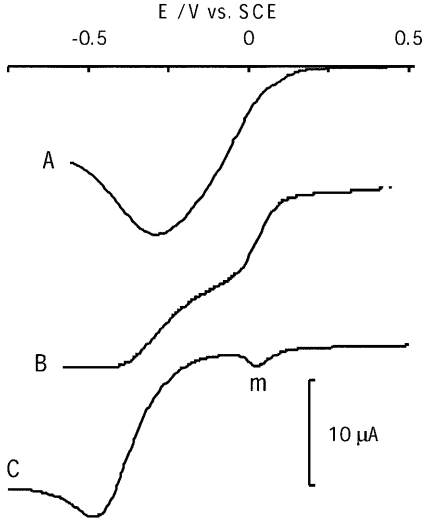

Fig. 6 Voltammetric peaks of heterogeneous samples of Li–Fe-Mn–O spinels. *A* C961 (single phase); *B* C965 (two-phase sample); *C* C1072 with 6% Li_2MnO_3 (m). Conditions: as in Fig. 4

Discussion

The electrochemical reactivity of Li–Fe–Mn–O spinels depends on their phase composition, ionic distribution, and particle size. All these influences could, in principle, be used for their electrochemical analysis, particularly for characterization of large series of synthetic samples with similar composition. We already proposed electrochemical dissolution as a tool to evaluate the quality of synthetic samples of Fe oxides as for the uniformity of their phase composition and particle size [32]. From the point of view of electroanalysis, Li–Fe–Mn oxides have several advantages over pure Fe oxides. The reactivity of the Li–Fe–Mn–O spinels studied changes with changing Fe/(Fe + Mn) ratio over a surprisingly wide range of 1 V in the voltammetric peak potentials, $LiFe_5O_8$ and Li–Mn–O spinels are almost ideally miscible, and in addition both the end members are electrochemically dissolved in the same supporting electrolyte. Another reaction of Li–Fe–Mn–O spinels, which can easily be monitored using voltammetry, is the electrochemically highly reversible Li^+ insertion/extraction reaction, for which the Mn valence and the amount of Li in the

tetrahedral position are essential. This reaction proceeds in an aqueous environment, which means a substantial technical simplification with respect to the nonaqueous solutions and inert and dry atmosphere, which is otherwise used to characterize Li–Mn–O spinels for Li^+ batteries [24].

Several authors proposed electrochemistry as a tool for characterization of inorganic materials [16, 33, 40, 41]. For many reasons the empirical electrochemical analysis has only exceptionally succeeded in competition with XRD analysis, spectroscopic methods, and other more common techniques. The exceptions are conditioned by an unusually well defined electrochemical reaction responsible for the easily measured characteristics, such as the peak potential. Moreover, electrochemical analysis is meaningful only if the solids are poorly crystalline, if they form continuous solid solutions with similar lattice parameters [35], or if their electrochemical characterization is explicitly required [18, 24]. Here, in the case of electrochemical dissolution of Li–Fe–Mn–O spinels the necessary well-defined reaction can be the reductive dissolution according to Eq. (5) and the easily measurable quantity is then the peak potential. We showed the problem of XRD analysis of solid solutions of nonstoichiometric spinels and mixtures of the spinel species with very similar lattice parameters. Voltammetry is here more sensitive to Fe/(Fe + Mn) heterogeneity than XRD.

The influence of the mean particle size on the dissolution peak potential was demonstrated for the example of the Li–Mn–O spinel in Fig. 4. It is well known that a bimodal distribution of particle sizes, i.e., the presence of a significant fraction of much smaller or much bigger particles beside the main size fraction, distorts the shape of the voltammetric peak as reported for ion insertion into cyanometallates [37] and dissolution of iron oxides [38, 39]. Nonuniform distribution of metals in solid solutions of α-$(Cr,Fe)_2O_3$ caused the splitting of the oxidative dissolution peak of those samples, which also exhibited broadened XRD lines [30], and we observed the same phenomenon for the nonuniform distribution of Fe/Mn in the Li–Fe–Mn–O spinels. The importance of the Fe/Mn ratio for the dissolution reactivity is clear from Fig. 5A and B. The phase specificity of the electrochemical dissolution of oxides of Fe [32], Cr [29], and Mn [15] was already described. Hence if some of these characteristics, i.e., particle size and elemental and phase composition, are not uniform, the voltammetric dissolution peak of these oxides will be widened, distorted, or even split as in the cases shown in Fig. 6.

Another reaction of the Li–Fe–Mn–O spinels, which is much more specific to their spinel structure, is the two-step Li^+ insertion/extraction. The peak shape is a more complex function of the sample crystallinity, with the valence being the most important characteristic. Unfortunately the structural nature of the two reaction steps is not clear and so the phenomenon cannot be directly related to the physicochemical characteristics of the samples.

Conclusions

Voltammetry of immobilized microparticles is a technique suitable for electroanalysis of Li–Fe–Mn–O spinels using irreversible reductive dissolution or the reversible Li^+ insertion/extraction reaction. Both reactions proceed in aqueous solutions at ambient atmosphere. Similarly to other well-defined dissolution reactions of metal oxides, each single-phase sample yields a single voltammetric dissolution peak without shoulders or more maxima. Li–Fe–Mn–O spinels behave as ideal solid solutions between $LiFe_5O_8$ and Li–Mn–O spinel, yielding a monotonous dependence of the potentials of reductive dissolution on the Fe/(Fe + Mn) ratio within a surprisingly wide range of about 1 V. Li^+ ion insertion/extraction proceeds easily only for Fe/(Fe + Mn) < 0.4 and the shape of the voltammetric peak reflects the crystallinity of the samples in a complex manner.

References

1. Le Cras F, Strobel P, Anne M, Bloch D, Soupart J-B, Rousche J-C (1996) Eur J Solid State Inorg Chem 33:67
2. Blasse G (1965) Philips Res Rep 20:528
3. Bonsdorf G, Schäffer K, Langbein H (1997) Eur J Solid State Inorg Chem 34:1051
4. Wolska E, Piszora P, Darul J, Nowicki W (2000) Mater Sci Forum (in press)
5. Wolska E, Stempin K, Krasnovska-Hobbs O (1997) Solid State Ionics 101–103:527
6. Piszora P, Stempin K, Wolska E (2000) Mater Sci Forum 321–324:796
7. Zinovik MA (1984) Zh Neorg Khim 29:1811
8. Endres P, Fuchs B, Kemmelr-Sack S, Brandt K, Faust-Becker G, Praas HW (1996) Solid State Ionics 89:221
9. Sano T, Tamaura Y (1999) Mater Res Bull 34:389
10. Volkhin VV, Leontieva GV, Onorin SA (1973) Neorg Mater 9:1041
11. Kanoh H, Feng Q, Miyai Y, Ooi K (1993) J Electrochem Soc 140:3162
12. Ohzuku T, Kitagawa M, Hirai T (1990) J Electrochem Soc 137:769
13. Tarascon JM, Guyomard D (1991) J Electrochem Soc 138:2864
14. Li W, Dahn JR (1995) J Electrochem Soc 142:1742
15. Bakardjieva S, Bezdička P, Gygar T, Vorm P (2000) J Solid State Electrochem 4:306
16. Scholz F, Meyer B (1998) In: Bard AJ, Rubinstein I (eds) Electroanalytical chemistry, a series of advances, vol 20. Dekker, New York, p 1
17. Lee JA, Maskell WC, Tye FL (1977) J Electroanal Chem 79:79
18. Fiedler DA, Besenhard JO, Fooken MH (1997) J Power Sources 69:157
19. Waki S, Dokko K, Itoh T, Nishizawa M, Abe T, Uchida I (2000) J Solid State Electrochem 4:205
20. Totir DA, Cahan BD, Scherson DA (1999) Electrochim Acta 45:161
21. Wolska E, Piszora P, Stempin K, Catlow CRA (1999) J Alloys Comp 286:203
22. Oak HN, Baek KS, Yu KS (1998) J Phys Condens Matter 10:1131
23. Mohan Rao M, Jayalakshmi M, Schäf O, Wulff H, Scholz F (1999) J Solid State Electrochem 4:17
24. Choy J-H, Kim D-H, Kwon C-W, Hwang S-J, Kim Y-I (1999) J Power Sources 77:1

25. Kanoh H, Feng Q, Miyai Y, Ooi K (1995) J Electrochem Soc 142:702
26. Kanamura K, Naito H, Yao T, Takehara Z-I (1996) J Mater Chem 6:33
27. Song MY, Ahn DS, Kang SG, Chang SH (1998) Solid State Ionics 111:237
28. Kawai H, Nagata M, Kageyama H, Tukamoto H, West AR (1999) Electrochim Acta 45:315
29. Grygar T, Bezdička P (1998) J Solid State Electrochem 3:31
30. Grygar T, Bezdička P, Caspary E-G (1999) J Electrochem Soc 146:3234
31. Bakardjieva S, Bezdička P, Grygar T, Vorm P (2000) In: Bezdička P, Grygar T (eds) Book of abstracts of solid state chemistry 2000. The Institute of Inorganic Chemistry, Academy of Sciences of the Czech Republic, Prague, p 124
32. Grygar T (1995) Coll Czech Chem Commun 60:1261
33. Brainina KZ, Vydrevich MB (1981) J Electroanal Chem 121:1
34. Bond AM, Scholz F (1991) Langmuir 7:3197
35. Jayrama-Reddy S, Dostál A, Scholz F (1996) J Electroanal Chem 403:209
36. Schwudke D, Stösser R, Scholz F (2000) Electrochem Commun 2:301
37. Schöder U, Scholz F (2000) Inorg Chem 39:1006
38. Mouhandess MT, Chassagneux F, Vittori O, Accary A, Reeves RM (1984) J Electroanal Chem 181:93
39. Grygar T (1996) J Electroanal Chem 405:117
40. Brainina KZ, Neyman E(1993) Electroanalytical stripping methods. Wiley, New York
41. Rusling JF, Suib SL (1994) Adv Mater 6:12